Biosensors and Bioelectronics 133 (2019) 160–168

Contents lists available at ScienceDirect

Biosensors and Bioelectronics

journal homepage: www.elsevier.com/locate/bios

# An electrochemical biosensor based on Hairpin-DNA modified gold electrode for detection of DNA damage by a hybrid cancer drug intercalation

Katherine Lozano Untiveros[a,b], Emanuella Gomes da Silva[a], Fabiane Caxico de Abreu[a], Edeildo Ferreira da Silva-Júnior[c], João Xavier de Araújo-Junior[c], Thiago Mendoça de Aquino[a], Stephanie M. Armas[b], Ricardo Olímpio de Moura[d], Francisco J.B. Mendonça-Junior[d], Vanessa Lima Serafim[d], Karin Chumbimuni-Torres[b,*]

[a] Chemistry and Biotechnology Institute (IQB), Federal University of Alagoas (UFAL), Campus A.C. Simões, Tabuleiro dos Martins, Maceió, AL, 57072-970, Brazil
[b] University of Central Florida. NanoBioelectrochemistry Laboratory, Department of Chemistry, University of Central Florida, 4000 Central Florida Blvd., Orlando, FL 32816, United States
[c] Nursing and Pharmacy School (ESENFAR), Federal University of Alagoas (UFAL), Campus A.C. Simões, Tabuleiro dos Martins, Maceió, AL, 57072-970, Brazil
[d] Laboratory of Synthesis and Drug Delivery, State University of Paraíba (UEPB), Campus V, 58071-160 João Pessoa, PB, Brazil

ARTICLE INFO

*Keywords:*
Stem-loop DNA (SL-DNA)
Double-stranded DNA biosensor
DNA damage
Hybrid acridine-thiophene anticancer drug
Gold electrode

ABSTRACT

An efficient and new electrochemical biosensor for detection of DNA damage, induced by the interaction of the hybrid anti-cancer compound (7ESTAC01) with DNA, was studied by differential pulse voltammetry (DPV). The biosensor consists of a Stem-Loop DNA (SL-DNA) probe covalently attached to the gold electrode (GE) surface that hybridizes to a complementary DNA strand (cDNA) to form a double-stranded DNA (dsDNA). The interaction and DNA damage induced by 7ESTAC01 was electrochemically studied based on the oxidation signals of the electroactive nucleic acids on the surface of the GE by DPV. As a result, the SL-DNA/GE and dsDNA/GE were tested with the reduced 7ESTAC01, showing the voltammetric signal of guanine and adenine, increase in the presence of 7ESTAC01. Under optimum conditions, the dsDNA/GE biosensor exhibited excellent DPV response in the presence of 7ESTAC01. The bonding interaction between 7ESTAC01 and *calf thymus* DNA (ctDNA) was confirmed by UV–Vis absorption spectroscopy, dynamic simulations (performed to investigate the DNA structure under physiological conditions), and molecular docking. Theoretical results showed the presence of hydrogen bonding and intercalation in the minor groove of DNA, involving hydrophobic interactions.

## 1. Introduction

Deoxyribonucleic acid (DNA) is considered the building block for genetic information. As such, DNA is also susceptible to chemical modifications via oxidation/reduction pathways, or interaction with small molecules (Arnold et al., 2015). Electrochemical detection of DNA interaction with small molecules has also been applied in the design of novel pharmaceutical drugs (Vyskočil et al., 2010; Aydoğdu et al., 2014).

A variety of small molecules are known to interact with DNA non-covalently through (i) groove binding interactions, (ii) electrostatic interactions, or (iii) intercalations between the stacked base pairs of the double-stranded DNA (Kovacic and Wakelin, 2001; Kalanur et al., 2009). Vibrational spectroscopy, fluorescence spectroscopy, surface plasmon resonance and nuclear magnetic resonance are just a few of the techniques employed to investigate the binding modes, thermodynamic properties and DNA affinity to these small molecules (Rauf et al., 2005). Unfortunately, these techniques mostly address the issues of structural analysis and binding mechanisms, rather than investigating DNA damage and its impact. Electrochemical biosensors, on the other hand, have been efficiently used to monitor the production of DNA damage via small molecule interaction (Lucarelli et al., 2004; Vyskočil et al., 2010). An electrochemical DNA biosensor is preferred due to the highly conducting ability provided by π-stack of nitrogenous bases, versatility to optimize DNA immobilization on an electrode surface, and ability to determine DNA damage induced by drug intercalation or via drug-induced oxidative stress (Labuda et al., 2009; Nepali et al., 2014; Arnold et al., 2015; Huang et al., 2016).

Oxidation of electroactive nucleic acids have been used to monitor DNA lesions on modified gold, glassy carbon and mercury electrodes (Paleček et al., 1998; Li et al., 2010; Ibañez et al., 2015). Benvidi et al. employed Au-thiol chemistry to covalently bind a stem-loop (SL)-DNA

* Corresponding author.
*E-mail address:* Karin.ChumbimuniTorres@ucf.edu (K. Chumbimuni-Torres).

https://doi.org/10.1016/j.bios.2019.02.071
Received 18 December 2018; Received in revised form 14 February 2019; Accepted 28 February 2019
Available online 14 March 2019
0956-5663/ 

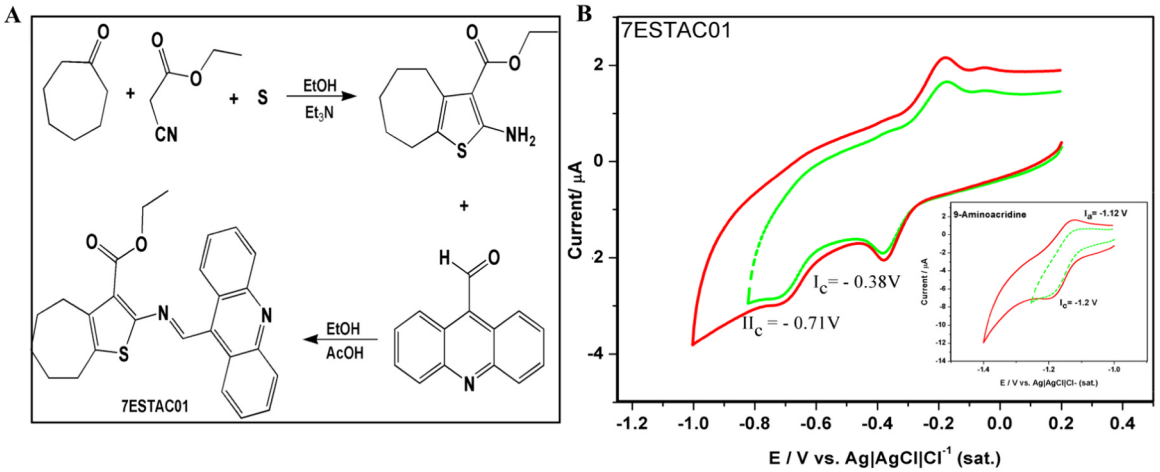


**Fig. 1.** Electrochemical characterization of 7ESTAC01 A) Chemical mechanism of synthesis of 7ESTAC01: Acridine-9-carboxaldehyde with 2-aminothiophene. B) Cyclic voltammogram of 10 mM 7ESTAC01 in mixture of pH 7.2, aqueous phosphate buffer and 20% DMF at a GE, with an Ag/AgCl reference electrode (RE), and the scan rate 0.1 V $s^{-1}$, E = potential, V = volt, A = ampere. Cyclic voltammogram of 10 mM 9-aminoacridine (B, inner graph*). (*) Red line represents the first scan. The green line represents the second scan with the potential range adjusted only to get the peak already registered on the first scan. (For interpretation of the references to color in this figure legend, the reader is referred to the web version of this article).

probe and 6-mercapto-1-hexanol (MCH) to form self-assembled monolayer on gold surfaces (Benvidi et al., 2015). MCH played a significant role in the overall optimized response of the DNA biosensor by avoiding non-specific DNA adsorption and adjusting the interfacial electron transfer on the electrode (Mills et al., 2017; McEwen et al., 2009). A Stem-Loop DNA (SL-DNA) structure offers higher thermodynamic stability when compared to a linear DNA structure. That stability could be explained by the presence of the hairpin loop with a reduced negative charge, which reduces the non-specific binding at the loop without compromising the first binding on the stem (Nguyen and Wilson, 2009).

The hybrid drug, a combination of two pharmacophores, has the potential to improve binding affinity, selectivity, and synergic activity towards nucleic acids (Goodell et al., 2006; Cholewiński et al., 2011; Nepali et al., 2014; Harbinder et al., 2017). Recent research has also investigated the amplification of oxidative stress in relation to DNA damage caused by sulfur, thiophene, triazole and acridine moieties (Brett et al., 2003; Pontinha et al., 2013; Sazhnikov et al., 2013; Noh et al., 2015; Deng et al., 2017). Acridine derivatives are highly interesting chemotherapeutic agents, which are linked to different pharmacophores in order to modify reactivity. Modifications of substituent groups in acridine derivatives have been found to further enhance the anti-cancer drug efficacy (Putic et al., 2010; Lafayette et al., 2013).

Here, we developed a highly sensitive electrochemical biosensor based on an SL-DNA probe that can detect DNA damage via hybrid drug, 7ESTAC01 interaction. 7ESTAC01 is composed of two anti-cancer pharmacophores, acridine, and thiophene. A complementary DNA strand (cDNA) was introduced to hybridize the SL-DNA probe to form a double-stranded DNA (dsDNA) biosensor. The optimization of SL-DNA/GE and dsDNA/GE modified electrode for sensitive detection of DNA damage was assessed by DPV and cyclic voltammetry (CV).

The present work involves two sections. First, we investigated the electrochemical oxidation of SL-DNA probe and dsDNA on the surface of the gold electrode induced by the presence of 7ESTAC01 to detect DNA damage by DPV. Second, the interaction of 7ESTAC01 with DNA was analyzed via UV–Vis absorption spectroscopy, *in-silico* dynamic simulations, and molecular docking.

## 2. Experimental section

### 2.1. Chemicals and reagents

All solutions were prepared with Milli-Q water using a Siemens PURELAB Ultra system (Lowell, USA). The immobilization buffer (IB) contains 50 mM Sodium Phosphate (Monobasic/Dibasic), 250 mM NaCl at pH 7.4. Hybridization buffer (HB) contains 50 mM Tris-HCl, 25 mM NaCl, 50 mM $MgCl_2$ at pH 7.4. Stock solutions of 1 mM 7ESTAC01 were prepared in HB and were evaluated in acetate solution at different concentrations. 1.0 M Acetate buffer solution at pH 4.2 was used for the DNA oxidation in presence of the 7ESTAC01. The Tris-HCl buffer was used for UV–Vis measurements and contains 50 mM NaCl, 5 mM, Tris-HCl at pH 7.2. The pH was adjusted with either NaOH or HCl solution. The *calf thymus* DNA (ctDNA) was prepared from dissolution of 12 mg $mL^{-1}$ in acetate buffer (pH 4.2; 1.0 M). This stock solution was kept at 8 °C for 24 h and stirred at certain intervals to ensure homogeneity of the final DNA solution. Trizma hydrochloride (Tris-HCl), tris (2-carboxyethyl) phosphine hydrochloride (TCEP), sodium phosphate dibasic ($Na_2HPO_4$), sodium phosphate monobasic dihydrate ($NaH_2PO_4{\cdot}2H_2O$), 6-mercapto-1-hexanol (MCH) and magnesium chloride ($MgCl_2$) were purchased from Sigma-Aldrich. Sodium chloride (NaCl), potassium chloride (KCl), sodium hydroxide (NaOH) and sulfuric acid ($H_2SO_4$) were obtained from Fisher Scientific (Pittsburgh, USA).

Gold electrodes (GEs) were purchased from CH Instruments (Austin, USA). Alumina slurry (1.0, 0.3 and 0.05 µm) was obtained from Buehler (Lake Bluff, USA). SL-DNA Probe, modified with a methylene-blue (MeB) redox marker (SL-DNA-MeB, **5´** -C6-S-S-TC GCG ACA TAC AAT AGA TCG CG-MeB-**3′**), and complementary DNA (cDNA, **5´**-CGA TCT ATT GTA TGT TAA CG −**3′**) were obtained from Biosearch Technologies, Inc. (Petaluma, USA) and used as received.

### 2.2. Synthesis of 7ESTAC01

The synthesis of 7ESTAC01 was synthesized at the Laboratory of Synthesis and Drug Delivery (LSVM) at the State University of Paraiba, Brazil. In short, as represented in Fig. 1A, the compound was obtained by reacting acridine-9-carboxaldehyde with 2-amino-thiophene moiety previously obtained via the classic Gewald reaction (Gewald, 1965; Gewald et al., 1966). Subsequent purification steps and recrystallization in ethanol yielded 7ESTAC01 as a red powder, with a melting point of 155–158 °C. Comparison of physical-chemical characteristics and spectral data confirms the achievement of the hybrid.

### 2.3. Preparation and immobilization of SL-DNA/GE and dsDNA/GE

GEs were used as substrate for SL-DNA probe and dsDNA immobilization. GEs were cleaned in a piranha solution (1:3 ratio of $H_2O_2$: $H_2SO_4$) and then polished on a micro cloth with 1.0 μm, followed by 0.3 and 0.05 μm alumina slurry. The GEs were then sonicated in water and ethanol to remove any residual alumina particles trapped at the surface of the electrode. The GE was activated in 0.5 M $H_2SO_4$ via CV from + 0.1 to + 1.6 V at a scan rate of 0.5 V $s^{-1}$.

The SL-DNA probe was immobilized on the electrode surface via a gold-thiol bond. The disulfide bonds of the SL-DNA probe were reduced with 1 mM TCEP by shaking the solution at room temperature for 1 h. The solution was then diluted with IB to yield 0.1 μM and 1.0 μM of the SL-DNA probe. 15 μL of this solution was drop casted onto the electrode and incubated at room temperature for 30 min. The electrodes were rinsed with IB and dried with nitrogen. To minimize nonspecific adsorption on the electrode surface, 15 μL of 2 mM MCH in IB was dropcasted on the electrode and incubated for 30 min. Then, the electrodes were rinsed with IB and dried with nitrogen. For dsDNA/GE preparation, SL-DNA modified GE was hybridized by dropcasting 15 μL of 50 nM cDNA in HB for 1.5 h at room temperature, which formed dsDNA at the surface of GE. Following hybridization, the GEs were rinsed using HB and then dried with nitrogen.

### 2.4. Optimization of 7ESTAC01 concentration and experimental timing

The protocol for analysis for the proposed biosensors consists of the following steps: (i) measurement of 7ESTAC01 signal in acetate buffer pH = 4.2; (ii) measurement of guanine and adenine signal obtained from SL-DNA/GE and dsDNA/GE modified electrode before the interaction with 7ESTAC01; (iii) measurements of guanine and adenine signal after interaction between 7ESTAC01 and DNA/GE (7ESTAC01-DNA complex). The optimization of 7ESTAC01 concentration was performed at various final concentrations of 10 μM, 100 μM, and 400 μM. Intercalation time of the compound with the SL-DNA/GE and dsDNA/GE was varied from 1 h, 2 h and 24 h.

### 2.5. Electrochemical measurements

Electrochemical measurements were performed with a CHI660D Electrochemical workstation (CH Instruments, USA) at room temperature. A typical 3-electrode system was used where the GE served as the working electrode, a platinum wire was used as the counter electrode (CE), and Ag/AgCl (3 M KCl) was used as a reference electrode (RE). The electrochemical characterization of 7ESTAC01 was investigated using CV in 0.2 M Phosphate buffer (pH = 7.2) and 20% Dimethylformamide (DMF) in nitrogen saturated solutions (the solubility of the hybrid compound in DMF gave better solubility for the analyses in protic media). CVs of 10 mM 7ESTAC01 were recorded from − 1.2 to + 1.0 V vs. Ag/AgCl at scan rates of 0.1 V $s^{-1}$.

CV was performed to analyze the electrochemical behaviour of SL-DNA probe and dsDNA immobilized on the GE and were recorded from 0.1 to 800 V $s^{-1}$ scan rates. The Optimization of SL-DNA/GE and dsDNA/GE focused on the analysis of the signal of suppression (% SS) before and after the hybridization with the cDNA. The % SS was calculated using the equation (Eq. (1)) (Lai et al., 2013) as follows:

$$\%\ SS = (I - I_0)/I_0 \times 100 \quad (1)$$

where $I$, is the current obtained upon hybridization with the cDNA and $I_0$ is the current obtained of the immobilized SL-DNA. We analyzed % SS of 0.1 μM and 1.0 μM SL-DNA probe concentration with a fixed 50 nM cDNA to obtain the dsDNA/GE biosensor.

The electro-oxidation of 7ESTAC01 and detection of DNA damage were conducted after the interaction of 7ESTAC01 with the SL-DNA/GE and dsDNA/GE using DPV. The oxidation of 7ESTAC01 and simultaneous determination of DNA damage was performed in acetate buffer at pH 4.2 using oxidation potentials from 0 to + 1.6 V; 0.05 V amplitude; 0.0167 s sample width; 0.5 s pulse period and 2 s quiet time. All the intercalation measurements of 7ESTAC01 and DNA/GE biosensors were done with 7ESTAC01 in solution. The reduction of 7ESTAC01 was performed in acetate buffer at a potential range from 0.0 to − 0.122 V for 100 s before the oxidation process.

### 2.6. Interaction of ctDNA with 7ESTAC01 by UV–Vis spectroscopic and molecular docking studies

UV–Vis absorption spectroscopy was performed at a fixed 20 μM 7ESTAC01 while varying ctDNA from 0 to 20 μM. The concentration of the stock solution of ctDNA (0.38 mM per nucleotide) was determined by UV absorption, using a molar extinction coefficient of 6600 $M^{-1}$ $cm^{-1}$ at 260 nm. A ratio > 1.8 at $A_{260}/A_{280}$ was obtained as indicative that DNA was sufficiently free of proteins. The intrinsic binding constant ($K_b$) of the compounds with ctDNA was calculated according to Wolfe-Shimer equation (Eq. (2)) (Sirajuddin et al., 2013) as follows:

$$\frac{[DNA]}{(\varepsilon_a - \varepsilon_f)} = \frac{[DNA]}{(\varepsilon_b - \varepsilon_f)} + \frac{1}{K_b(\varepsilon_b - \varepsilon_f)} \quad (2)$$

where [DNA] is the concentration of DNA per nucleotides, $\varepsilon_a$ is the molar absorption coefficient of the complex at a given DNA concentration ($A_{obs.}$ / [Compound]), $\varepsilon_f$ is the molar absorption coefficient of the complex in free solution, and $\varepsilon_b$ is the molar absorption coefficient of the complex when fully bound to DNA. A plot of equation (Eq. (2)) allows the determination of the intrinsic binding constant $K_b$, obtained by the linear data fit. The value of constant was calculated as the ratio between the slope and the intercept.

All molecular dynamic and Density Function Theory (DFT) calculations were performed in agreement with Silva et al., (2016, 2017). The coordinates for building the molecular model were extracted from the X-ray crystal structure of the *ct*DNA dodecamer d(CGCGAATTC GCG) (PDB entry: 1BNA). Gold v.5.4 software from Cambridge Crystallographic Data Centre (CCDC) was utilized to perform all molecular docking studies (Huang et al., 2013). Initially, all hydrogens were added into the DNA structure and, then, 7ESTAC01 (ligand) was introduced into space. Different genetic algorithms (GA) were applied to find the best score function for the ligand. The GoldScore, ChemScore, Piecewise Linear Potential (ChemPLP), and Astex Statistical Potential (ASP) functions were employed to obtain the best 10 binding poses for the ctDNA-7ESTAC01 complex. All search coordinates were manually introduced, as $x$: 1.389, $y$: − 1.149, and $z$: − 7.376 Å (Murali et al., 2017).

After the docking calculations, the DFT calculations were performed using quantum mechanics (QM) models from the Spartan'14 program to determine the corrected free binding energy ($\Delta G$) for the ctDNA-7ESTAC01 complex. The potential of intercalation of 7ESTAC01 was investigated by theoretical methods. The optimized geometries of this compound's ability to interact with the ctDNA were taken from docking analysis. In addition, the coordinates of the ctDNA structure were taken from the crystal structure (PDB ID: 1BNA), and the ligand and water molecules were removed. The binding energy of the DNA/ligand complex was calculated by applying the M06/6-31G (d) basis set. The M06 method employed the global hybrid functional, which is the top performer within the 6 functionals of the main group, thermochemistry, kinetics and non-covalent interactions. Moreover, frequency calculations were performed to confirm the nature of the stationary point at the same level. QM binding energies were obtained applying the

following formula, in which the free binding energy of Gibbs ($\Delta G$) was calculated as the difference between the energy of the complex ($E_{DNA\text{-}ligands}$) and the sum of the ctDNA ($E_{ctDNA}$) and ligand ($E_{ligand}$) energies based on the equation (Eq. (3)).

$$\Delta G = [E_{DNA-ligands} - (E_{ctDNA} + E_{ligand})] \quad (3)$$

The final energy of the optimized structure was improved by including the single point energy from the 6-31G(d) basis set unscaled zero-point energy (ZPE) and thermal corrections (at 298.15 K and 1 atm) estimated at the same level of theory, using the Spartan'14 program. All these protocols were performed exactly as described by Silva-Júnior et al. (2017).

## 3. Results and discussion

### 3.1. Electrochemical characterization of 7ESTAC01

The electrochemical characterization of acridine-9-carboxaldehyde with 2-aminothiophene derivative designed as 7ESTAC01 (Fig. 1A) was investigated using CV on the GE in a mixture of phosphate buffer (pH 7.2) and 20% DMF in nitrogen saturated solutions. CVs were registered in the range from − 1.8 V to + 1.0 V (Fig. 1B). Fig. 1B shows the reduction of 7ESTAC01 displaying two waves. The first one exhibits a quasi-reversible reduction peak at $E_{Ic} = -0.38$ V vs. Ag/AgCl with a peak separation potential (ΔE = Ea-Ec) of 150 mV. The second one displays an irreversible reduction peak at $E_{IIc} = -0.71$ V. In the same way, 9-aminoacridine, which was synthesized containing only acridine, was examined in the same potential range from − 1.8 V to + 1.0 V (Fig. 1B, inner graph). The first cathodic potential for the 9-aminoacridine showed a single peak at $E_{Ic} = -1.2$ V, Fig. 1B (inner graph). It is important to mention that no wave was registered in the oxidation potential range for the 9-aminoacridine. Thus, only the reduction potential range was further studied.

The reduction of 7ESTAC01 showed the first cathodic peak at $E_{Ic} = -0.38$ V, which was lower than the 9-aminoacridine alone. This behaviour hinted a possible synergic activity of 7ESTAC01 due to the significant shift of the first cathodic peak potential. It is worth mentioning that most of the bioactive compounds are recorded at a less negative potential of − 0.5 V (Bouffier et al., 2012; Dogan-Topal et al., 2014; Nepali et al., 2014; Noh et al., 2015). Thus, 7ESTAC01 represents a promising anti-cancer drug candidate; even though additional bioactivity tests must still be performed.

### 3.2. Characterization and optimization of SL-DNA/GE and dsDNA/GE

SL-DNA probe contains a thermodynamically stable structure and was used due of its capacity to detect specific site interaction (Nguyen and Wilson, 2009). Both SL-DNA and dsDNA structures were proposed and evaluated, as shown in Scheme 1. The SL-DNA probe, modified with MeB redox marker, was covalently attached to the gold electrode (GE) via a thiol bond (Scheme 1). The cDNA was added to hybridize the SL-DNA probe to form a dsDNA/GE (Scheme 1B). Here, CV was used to evaluate the electrochemical characterization, and subsequently optimization of SL-DNA and dsDNA immobilized on the surface of the GE (see Fig. S1 in the Supplementary information). Cyclic voltammograms of the SL-DNA probe in Fig. S1A and Fig. S1B show a high current for MeB due to the close proximity of the redox marker (MeB) to the electrode's surface in the SL-DNA configuration (Scheme 1), since it provides an efficient electron transfer. On the other hand, after hybridization with cDNA, the MeB is distant from the surface of the electrode (Scheme 1), consequently decreasing the current of MeB (Fig. S1A and B).

The signal suppression (% SS) as a surface coverage was further evaluated based on equation (Eq. (1)). The % SS of the dsDNA/GE based on 0.1 μM SL-DNA probe upon hybridization of cDNA, increased in relation to the scan rate, and plateaued around 94% at 100 V $s^{-1}$ (Fig. S1C). However, when the concentration was at 1.0 μM SL-DNA probe, the %SS reached its maximum at 92% and 600 V $s^{-1}$. This shows that the proximity of the MeB redox marker supported efficient electron transfer at significantly high scan rates (Fig. S1D). 1.0 μM SL-DNA probe was used to further characterize and optimize the SL-DNA/GE and dsDNA/GE biosensors.

### 3.3. Electrochemical behaviour of SL-DNA/GE and dsDNA/GE by Differential Pulse Voltammetry

The oxidative DNA damage could be induced in two ways (i) by electro-oxidation and (ii) via oxidizing agents that interact narrowly with DNA (Cadet and Wagner, 2013). Since DNA oxidation is the process of oxidative injury; in this experiment, the behaviour of SL-DNA/GE and dsDNA/GE was assessed only under electro-oxidation and without the presence of an oxidizing agent (7ESTAC01).

The electrochemical response for SL-DNA/GE and dsDNA/GE were first studied by DPV in acetate buffer at pH 4.2. The modified GE was used for the electrochemical oxidation of adenine (A) and guanine (G). As shown in Fig. 2A, both types of DNA modified GE exhibited peak currents at 1.04 V due to the guanine bases. No adenine peaks were observed for either sensor, which could be explained by the stability of the stem-loop DNA structure through the adenine electro-oxidation (Wei et al., 2011). Otherwise, the electro-oxidation process for modified GE reported oxidation peaks between + 0.85 V to + 0.96 V for guanine (Barman and Jasimuddin, 2014). The DPV peak potentials of the guanosine on the ssDNA and dsDNA in acetate buffer reported by Oliveira and Oliveira-Brett (2010) were in agreement with our values. Those results showed that the electrochemical current signal of SL-DNA probe and dsDNA on the GE were mainly attributed to the electrochemical oxidation of guanine bases, which was expected because guanine is the most readily oxidized of the DNA bases (McEwen et al., 2009). Similarly, the DPV peak current of guanine on SL-DNA/GE and dsDNA/GE were further evaluated. As indicated in Fig. 2A (inset), SL-DNA/GE, and dsDNA/GE showed a reproducible guanine peak current at 7.94 and 3.86 μA, respectively. The blank response of the GE does not show any peak. All measurements were conducted in triplicates. The S.D of the guanine peak current on the SL-DNA/GE and dsDNA/GE were 0.14 μA and 0.24 μA, respectively (Fig. 2A, inner graph).

The influence of the scan number to the oxidative DNA damage was subsequently examined as an indicator of consecutive DNA lesions under electro-oxidation. DNA oxidation is the process of oxidative injury, so it is expected to see higher oxidative damage to the DNA as the number of scans increases. Fig. 2B, prove this hypothesis, wherein the oxidation current of guanine increases with the number of scans, indicating that the electron donor was DNA itself.

Furthermore, for the dsDNA/GE, the presence of the intermediate form of 8-oxoguanine (8-oxoG) at E = + 0.25 V is a reliable indicator that the oxidation of guanine is taking place (Fig. 2B) from the second scan onwards. In addition, the guanine oxidation peak current increases as the oxidative DNA damage increases for dsDNA/GE.

### 3.4. Optimization of the concentration of 7ESTAC01 and detection of DNA damage

The electro-oxidation processes involved in purine DNA bases are similar to those affecting enzymatic oxidation. For this reason, the electro-oxidation of the DNA immobilized on the GE was applied to detect DNA damage through the interaction with the oxidizing compound (7ESTAC01). The oxidative DNA damage was induced by electro-oxidation in the presence of the given 7ESTAC01. A reduction potential was applied to 7ESTAC01 to obtain 7ESTAC01 radicals to

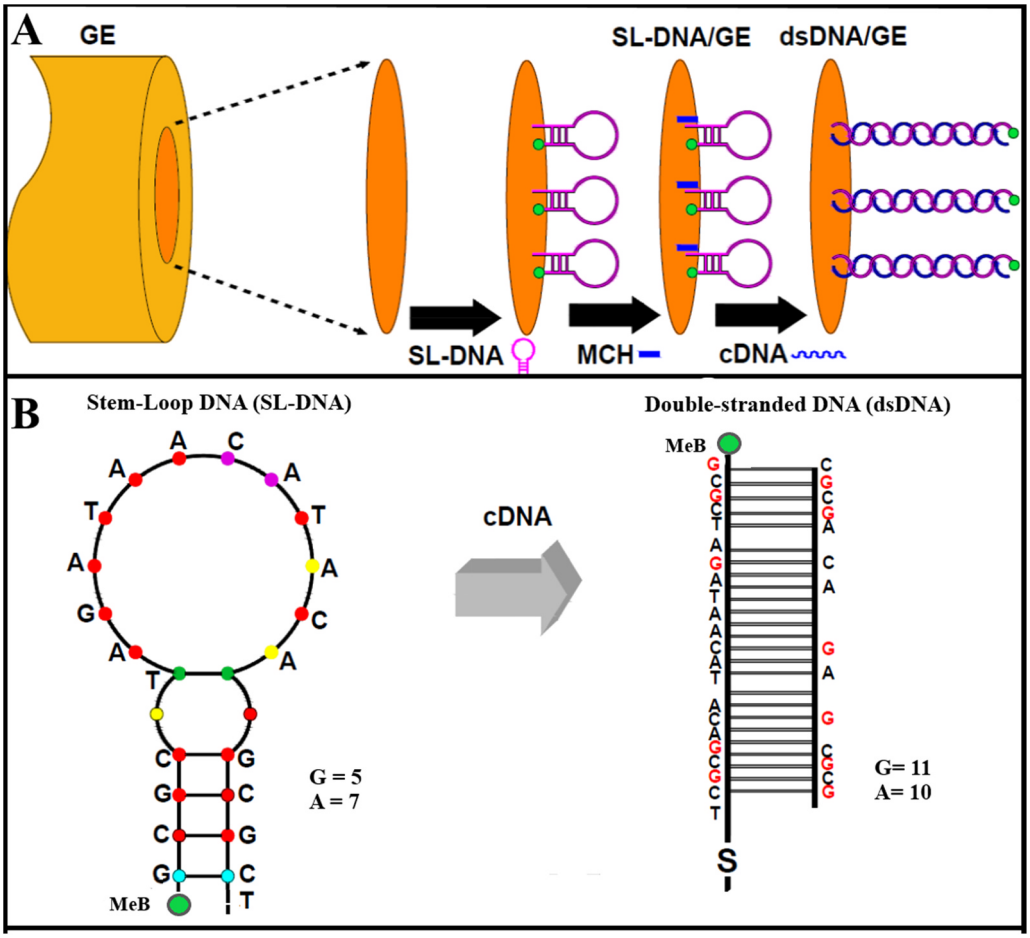


**Scheme 1.** Schematic representation the fabrication the Hairpin-DNA modified Gold electrode (GE). A) Schematic of the assay procedure of the SL-DNA probe and dsDNA biosensor at GE B) SL-DNA probe and dsDNA structures. SL-DNA probe, 5´-C6-S-S-TC GCG ACA TAC AAT AGA TCG CG-MeB-3′. The number of Guanines (G). The number of adenines (A). 6-mercapto-1-hexanol (MCH). Complementary DNA (cDNA). Methylene-blue (MeB).

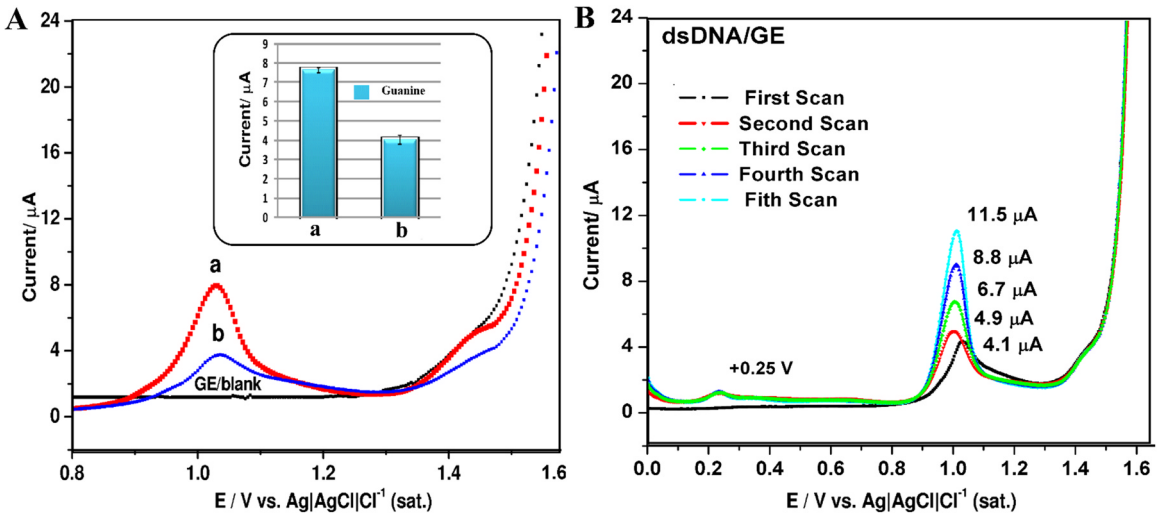


**Fig. 2.** Electrochemical behaviour of SL-DNA/GE and dsDNA/GE under electro-oxidation by DPV. (A) Comparison of DPV signals between SL-DNA probe (curve a) and dsDNA (curve b) and blank response of GE (GE/blank). Histogram graph represents the guanine peak current for SL-DNA/GE (a) and dsDNA/GE (b) modified electrode (A, inner graph). (B) DPV response for dsDNA/GE from first to the fifth scan. The electro-oxidation by DPV was carried out in acetate buffer at pH 4.2 for potentials range from 0.0 to + 1.6 V; amplitude 0.05 V; sample width 0.0167 s. (For interpretation of the references to color in this figure legend, the reader is referred to the web version of this article).

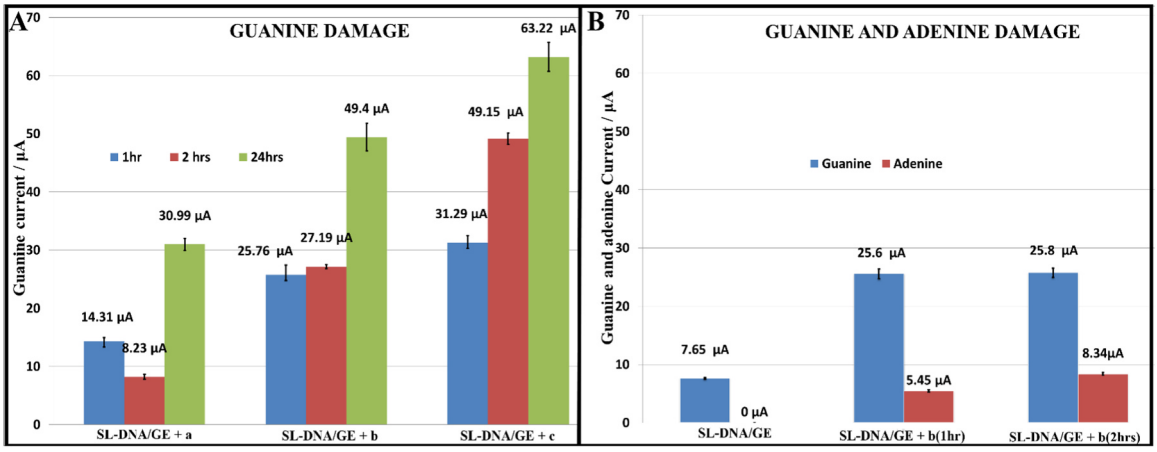


**Fig. 3.** DPV peak currents responses under electro-oxidation on SL-DNA/GE in the presence of 7ESTAC01 to the detection of DNA damage. (A) Guanine peak current in the presence of 7ESTAC01 at concentrations of (a) 10, (b) 100, (c) 400 µM for 1, 2 and 24 h of interaction. (B) Guanine (blue histogram on the left) and Adenine peak current (red histogram, on the right) in the presence of 100 µM 7ESTAC01 (b) for 1 and 2 h of interaction. Histograms represent the guanine and adenine peak current for SL-DNA/GE extrapolated from the DPV signal. Results were expressed as the average of three independent experiments. Error bars represent standard deviations. (*) All the intercalation measurements were done with 7ESTAC01 in solution. (For interpretation of the references to color in this figure legend, the reader is referred to the web version of this article).

damage DNA. According to Abreu et al. (2002) and Dogan-Topal et al. (2014) certain anticancer drugs require the formation of short-lived radicals to interact and damage DNA.

The direct determination of the oxidation of electroactive DNA bases in the presence of 7ESTAC01 were carried out by DPV from 0 to + 1.6 V. The oxidation peak current differences between SL-DNA/GE and their corresponding SL-DNA/GE-7ESTAC01 system were further investigated in acetate buffer (pH 4.2). The reproducibility of the SL-DNA/GE was investigated in presence and absence of different concentrations of 7ESTAC01 (Fig. 3A and B). As seen in Fig. 3A, 7ESTAC01 interactions with the SL-DNA/GE were examined at different times, 1, 2 and 24 h.

In general, the guanine oxidation peak current increased notoriously as the interaction time increased, which indicated the formation of SL-DNA/GE-7ESTAC01, increasing the electron transfer ability of the SL-DNA/GE. Another valuable data collected from Fig. 3A showed that the guanine oxidation peak current increased as the 7ESTAC01 concentrations increased. It is important to note that acridine, which binds to DNA by intercalation, might either donate electrons to or accept electrons from, the double helix, thus actively participating in electron transfer reactions (Kovacic and Wakelin, 2001; Baguley et al., 2003; Nepali et al., 2014). These results support literature data of acridine and its importance on the electron transfer (Noh et al., 2015); showing that oxidation of 7ESTAC01 is facilitating the electron transfer on the SL-DNA/GE biosensor. The adenine oxidation was evaluated with the minimum required concentration of 7ESTAC01 (Fig. 3B). The electrochemical oxidation of adenine followed a multiple step, six electron, six protons oxidation (Wei et al., 2011), which implies a more demanding oxidation process compared to guanine. As seen in Fig. 3B, the adenine oxidation was registered in the presence of higher concentrations of 7ESTAC01, equal to 100 µM 7ESTAC01 (Fig. 3B). Taking into account the interaction time of 1 and 2 h under the same level of 100 µM 7ESTAC01, adenine peak currents registered at 5.45 µA and 8.34 µA, respectively.

The reproducibility was evaluated for three different concentrations of 7ESTAC01 with 1, 2 and 24 h to obtain the best timing conditions for the interaction. After three successive measurements, the S.D of the guanine peak current on the SL-DNA/GE response to 10,100 and 400 µM 7ESTAC01 with 1 h of interaction were 0.67 µA, 1.70 µA and 1.19 µA, respectively. For the same conditions, the standard deviations of SL-DNA/GE response to 10, 100 and 400 µM 7ESTAC01 with 2 h of interaction were 0.44 µA, 0.33 µA and 0.98 µA. The S.D with 24 h of interaction for the same concentrations showed 1.01 µA, 2.36 µA and 2.51 µA, showing an acceptable reproducibility. Nevertheless, based on biosensor performance, the best S.D was obtained for 2 h of interaction. All further experimentation was carried out at the optimized two hours of interaction time.

### 3.5. Interaction of SL-DNA/GE and dsDNA/GE with 7ESTAC01 and detection of DNA damage

All the following experiments were carried out for different concentrations of 7ESTAC01 with 2 h of interaction time. As depicted in Fig. 4, after the addition of 7ESTAC01, the strong binding interaction between 7ESTAC01 with guanine and adenine base of SL-DNA/GE and dsDNA/GE occurred. Therefore, as the concentration of 7ESTAC01 increases, the oxidation peak current of SL-DNA probe and dsDNA increased (Fig. 4A and B). These results are similar to those obtained by Lucarelli et al. (2002). Lucarelli and co-workers utilized screen-printed electrodes for the detection of apolipoprotein E, where an increase of the electrochemical signal of the guanine base resulted from the non-specific interaction of the apolipoprotein E and the DNA immobilized on the electrode. The increasing oxidation peak current we report here is consistent with other electrochemical DNA/GE biosensors testing a redox-active intercalator, such as in the case of anthraquinone mono sulfonic acid (AQMS) (Wong and Gooding, 2006). Electron transfer from the DNA to AQMS intercalated into DNA duplexes reported the growth of the peak current signal with time. These last results support the electrochemical behaviour of our biosensors in the presence of 7ESTAC01, which is intercalated into the double-stranded DNA.

To evaluate the level of DNA damage with the dsDNA/GE and SL-DNA/GE, we compared guanine and adenine peak current in the same conditions. The adenine oxidation was recorded for SL-DNA/GE and dsDNA/GE, each yielding different sensitivity levels. The SL-DNA/GE-7ESTAC01 showed adenine oxidation for 100 µM (Fig. 3B) and 400 µM 7ESTAC01 (Fig. 4A). Notoriously, an adenine peak for 100 and 400 µM 7ESTAC01 (Fig. 4B, red histograms) with the dsDNA/GE-7ESTAC01, reached higher adenine peak current at 12.36 µA and 18.63 µA, respectively. On the other hand, as shown in Fig. 4 (blue histograms), the guanine oxidation was seen for dsDNA/GE and SL-DNA/GE with the presence of the minimum concentration of 7ESTAC01. The guanine peak current for 40 µM 7ESTAC01 with SL-DNA/GE and dsDNA/GE, reached 9.412 µA and 11.35 µA, respectively (Fig. 4A and B, inner graph). These results not only validated the strong interaction between 7ESTAC01 and purine bases but also emphasized the higher sensitivity

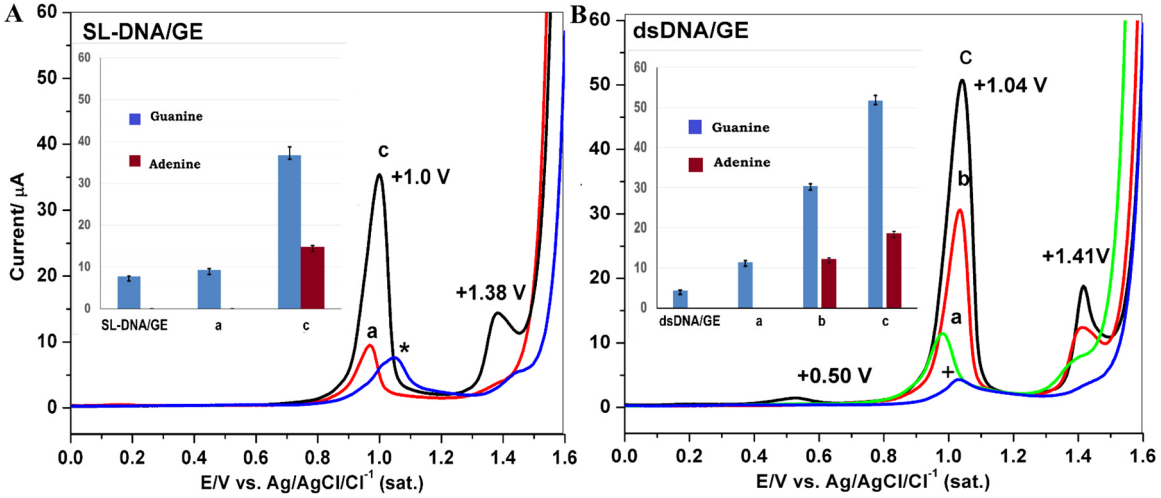


**Fig. 4.** Detection of the DNA damage product of the interaction between SL-DNA/GE and dsDNA/GE with 7ESTAC01 expressed by the DPV peak currents. DPV peak currents responses under electro-oxidation on SL-DNA/GE (A) and dsDNA/GE (B) in presence of 7ESTAC01 at concentrations of (a) 40, (b) 100 and (c) 400 µM for 2 h of interaction. Histograms represent the guanine and adenine peak current for SL-DNA/GE, and dsDNA/GE extrapolated from the DPV signal of each biosensor (A and B, inner graph). Error bars represent standard deviations (S.D). The S.D of the guanine peak current on the SL-DNA/GE for 40 and 400 µM 7ESTAC01 were 0.31 µA and 0.91 µA, respectively. The S.D of the guanine peak current on the dsDNA/GE for 40, 100 and 400 µM 7ESTAC01 were 0.44 µA, 0.52 µA and 1.32 µA, respectively. DPV signal in acetate buffer for SL-DNA/GE (*) and dsDNA/GE (+) without the presence of 7ESTAC01.

and more damage induced by employing the dsDNA/GE versus the SL-DNA/GE. The dsDNA and SL-DNA sequences exhibit 11 and 5 guanines, respectively. It is possible that 7ESTAC01-DNA intercalation can lead to breaking hydrogen bonds and exposing guanine and adenine bases to the surface of the GE. Therefore, it is likely that the higher oxidation peak current exhibited by the dsDNA/GE-7ESTAC01 system is due to a higher quantity of available guanine and adenine bases in comparison to the SL-DNA/GE-7ESTAC01 system (Fig. 4A). In fact, two critical parameters must be followed to improve the electron transfer efficiency, (i) type of DNA structure, and (ii) distance between guanine base and electrode surface (Brett et al., 2003; McEwen et al., 2009; Ibañez et al., 2015). Similar results were observed in a single stranded DNA modified GE biosensor, wherein electron transfer efficiency was the highest when guanine bases were in close proximity and exposed to the surface of the GE (Huang et al., 2016). In addition, the high charge migration along the DNA duplex in the presence of a DNA intercalator like 7ESTAC01, can also account for the higher oxidation peak current seen in the dsDNA platform (Liu and Barton, 2005; Elias et al., 2008).

The 8-oxoguanine (8-oxoG) is arguably the most important mutagenic lesion in DNA. The oxidation potentials are highly dependent on the type of electrode and pH of the solution. With that in mind, it has been reported an 8-oxoG oxidation peak at + 0.25 and + 0.45 V, for neutral (Ferapontova, 2004) and acidic pH (Oliveira and Oliveira-Brett, 2010), respectively. In the present study, the presence of the 8-oxoG at E = +0.5 V (Fig. 4B, black line) after the interaction with the highest concentration of 7ESTAC01 (400 µM) with the dsDNA/GE biosensor, demonstrates a substantial DNA damage.

To understand the mechanism behind the observed increase in peak current signal from purine bases in the presence of 7ESTAC01 radicals, another double-stranded ctDNA was immobilized by non-covalent bonding on a glassy carbon electrode (GCE) (Supplementary information). The double-stranded ctDNA is a natural DNA from *calf thymus* widely used in studies of DNA binding anticancer compounds. The damage of the ctDNA in the presence of 7ESTAC01 radicals was investigated in acetate buffer solution at pH 4.2 by DPV. Fig. S2 shows DPV peak potentials characteristic of the guanine and adenine bases at the GCE (Li et al., 2010; Aydoğdu et al., 2014). In the presence of 7ESTAC01 in solution, the peak current recorded a significant increase of guanine and adenine bases at + 1.03 V and + 1.29 V, respectively, which could imply the opening of the double helix of ctDNA (Fig. S2). Therefore, the increase in the signal, regardless of the electrode, indicates that the electron transfer through DNA increases in the presence of the 7ESTAC01 (oxidizing agent). It demonstrates that the 7ESTAC01 mechanism of intercalation into the DNA through electro-oxidation caused a substantial distortion of the double-stranded ctDNA. It also corroborates the imminent breaking of the double helix DNA, exposing the purine bases to the surface of the electrode as a result of the DPV current increase in the presence of 7ESTAC01. Finally, the blank signals upon oxidation of 7ESTAC01 were analyzed by DPV for both unmodified electrodes, GCE (Fig. S2) and the GE (Fig. S3) under the same working conditions. As recorded in Fig. S2 and Fig. S3, the blank response of the GE/GCE + 7ESTAC01 does not show any peak.

### *3.6. Interaction of DNA with 7ESTAC01 by UV–Vis spectroscopy, molecular docking and density function theory (DFT) studies*

Elucidating the binding between 7ESTAC01 and DNA provides help in understanding drug-DNA interactions and consecutive DNA damage on the surface of the GE. The interaction of an anticancer drug 7ESTAC01 with double-stranded ctDNA was studied using various approaches like UV–Vis spectroscopy, Molecular Docking, and Density Function Theory (DFT) studies.

UV–Vis spectroscopy confirmed 7ESTAC01-DNA interaction. Importantly, as depicted in Fig. 5A, the presence of an isosbestic point developed at 297 nm in the 7ESTAC01-DNA spectra indicates intercalation as a dominant binding mode. Moreover, UV–Vis showed a binding constant of $K_b = 6.57 \times 10^4$ L mol$^{-1}$ at 260 nm using the Wolfe-Shimer equation (Eq. (2)). The small molecules can interact with DNA involving a single mode of binding or mixed binding modes. Thus, the exact mode of interaction can be established merely by this technique due to the presence of the isosbestic point; however, another kind of non- covalent interactions could be present.

Other types of non-covalent interactions were further studied by Molecular Docking and DFT studies. For these studies, the GoldScore was selected as the best algorithm to predict results without large deviations between generated poses. Based on this, the GoldScore function was employed to determine different thermodynamic parameters related to the 7ESTAC01 compound (see Table S in the Supplementary information). From this analysis, the most important type of interaction can be identified and, consequently, it is possible to determine their

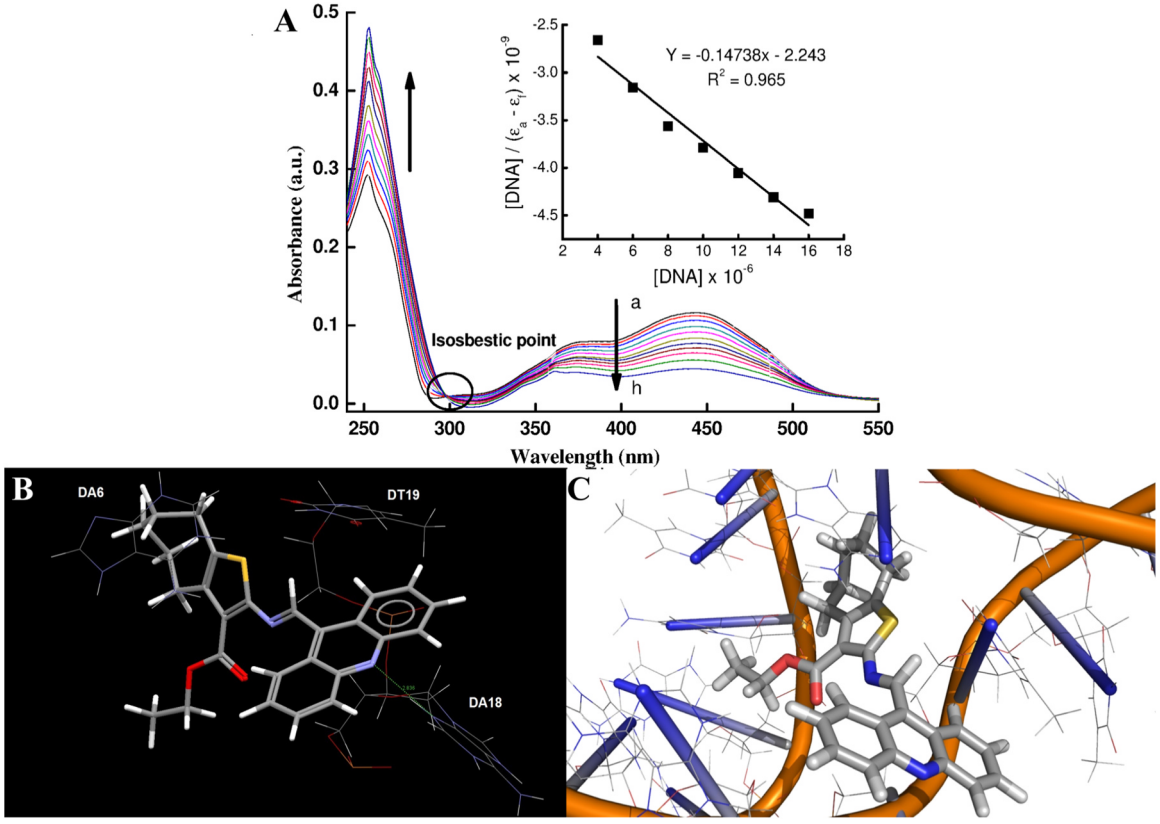


**Fig. 5.** Interaction of DNA with 7ESTAC01 by UV–Vis Spectroscopy, and Molecular docking. (A) UV–Visible absorption spectra of 20 μM 7ESTAC01 in presence of different concentrations of DNA (μM): (a) 0.0; (b)2; (c)10; (d)12; (e)14; (f)16; (g)18; (h)20. (B) Molecular docking of 7ESTAC01 (forward of the mage) to ctDNA (background structure) sites, represented by H-bond at DA18. (C) The binding pose of ctDNA (orange helix) acting via intercalation mechanism between the aminothiophene and acridine domains of 7ESTAC01. (For interpretation of the references to color in this figure legend, the reader is referred to the web version of this article).

contribution in kcal $mol^{-1}$ (Kamal et al., 2010; Arshad et al., 2017; Kundu and Chattopadhyay, 2017; Veerashekhar Goud et al., 2017). According to the quantitative results from the Molecular Docking and DFT studies (Table S), it is observed that significant interactions from the 7ESTAC01-DNA complex are the contributions of Van der Walls, 46.35 kcal $mol^{-1}$. In addition, it was observed that the 7ESTAC01 compound presented a significant external H-bond value of 1.2 kcal $mol^{-1}$. This happens due to 7ESTAC01's ability to form an H-bond with the NH donor from the adenine base (DA18), at a distance of 2.836 Å (Fig. 5B). After DFT calculations from ctDNA and 7ESTAC01 (free and binding), Gibbs free energy (ΔG) from the complex was low, suggesting a high affinity, showing its relation to the FitScore value, 63.44 (Table S). Therefore, binding of 7ESTAC01 analyzed via molecular docking (Fig. 5C), demonstrates that this compound could act via intercalation mechanism, considering that the aminothiophene and partially acridine rings are located between the DNA bases.

A careful analysis of the type of interaction between the hybrid 7ESTAC01 and the DNA represents the success of producing oxidative damage in the DNA. In this way, the interaction between DNA and 7ESTAC01 characterized by UV–Vis spectroscopy, Molecular Docking, and DFT studies showed that the 7ESTAC01 act via an intercalation mechanism into the DNA. Besides, the low free energy of Gibbs (ΔG) calculated from molecular docking suggests an excellent affinity 7ESTAC01-DNA.

## 4. Conclusions

Here, a novel electrochemical biosensor, divided into two configurations, SL-DNA/GE and dsDNA/GE, was optimized and characterized for detection of DNA damage caused by intercalation with a new hybrid anti-cancer drug (7ESTAC01). DPV analysis of guanine and adenine bases presented high sensitivity and efficiency of the SL-DNA probe modified GE and the dsDNA. High intercalation between DNA and 7ESTAC01 was determined to be a critical parameter to improve the sensitivity of the biosensor. DPV analysis of dsDNA in the presence of high concentration of 7ESTAC01 led to the formation of 8-oxoguanine, which is considered a key indicator of a mutagenic lesion in DNA. Intercalation mechanism was demonstrated using molecular docking, DFT studies, and UV–Vis Spectroscopy. These studies showed aminothiophene and partially acridine rings located between DNA bases, as well as an isosbestic point at 297 nm in the 7ESTAC01-DNA spectra, indicating the intercalation as a dominant binding mode.

The dsDNA/GE showed higher sensitivity in the presence of the 7ESTAC01 due to a higher quantity of purine bases in comparison to the SL-DNA by itself. The high sensitivity of this novel biosensor allows detection of minimal DNA damage and can be further expanded to study DNA damage with many other drugs.

## Supplementary information

Optimization of SL-DNA/GE and dsDNA/GE biosensor by Cyclic Voltammetry, electrochemical ctDNA biosensor on the Glassy Carbon Electrode, Detection of the DNA damage product of the interaction of ctDNA/GCE and 7ESTAC01, DPV signal of 7ESTAC01 on the Gold Electrode, Molecular Docking and DFT studies for 7ESTAC01 and calf thymus DNA. This material is available free of charge via the Internet.

## CRediT authorship contribution statement

**Katherine Lozano Untiveros:** Conceptualization, Methodology, Validation, Investigation, Writing - original draft, Writing - review & editing. **Emanuella Gomes da Silva:** Methodology, Writing - review & editing. **Fabiane Caxico de Abreu:** Conceptualization, Validation, Investigation, Writing - review & editing, Supervision, Funding acquisition. **Edeildo Ferreira da Silva-Júnior:** Methodology. **João Xavier de Araújo-Junior:** Methodology. **Thiago Mendoça de Aquino:** Methodology, Writing - review & editing, Supervision, Funding acquisition. **Stephanie M. Armas:** Validation, Investigation, Writing - review & editing. **Ricardo Olímpio de Moura:** Methodology. **Francisco J.B. Mendonça-Junior:** Methodology, Writing - review & editing. **Vanessa Lima Serafim:** Methodology. **Karin Chumbimuni-Torres:** Conceptualization, Validation, Investigation, Writing - review & editing, Supervision, Funding acquisition.

## Acknowledgements

This work is supported by Organization of American States (OAS) under the OAS-GCUB scholarship program (P.202.458.3000). Foundation for Research Support of the State Alagoas (FAPEAL), Brazil. NSF-CBET, United States, grant number #1706802 and Florida Department of Health Grant #7ZK05.

## Declaration of interests

None.

## Appendix A. Supporting information

Supplementary data associated with this article can be found in the online version at https://doi.org/10.1016/j.bios.2019.02.071.

## References

Abreu, F.C., Goulart, M.O.F., Oliveira Brett, A.M., 2002. Biosens. Bioelectron. 17, 913–919.
Arnold, A.C., Grodick, M.A., Barton, J.K., 2015. Cell Chem. Biol. 23, 183–197.
Arshad, N., Perveen, F., Saeed, A., Channar, P.A., Farooqi, S.I., Larik, F.A., Ismail, H., Mirza, B., 2017. J. Mol. Struct. 1139, 371–380.
Aydoğdu, G., Günendi, G., Zeybek, D.K., Zeybek, B., Pekyardımcı, Ş., 2014. Sens. Actuators B Chem. 197, 211–219.
Baguley, B.C., Wakelin, L.P.G., Jacintho, J.D., Kovacic, P., 2003. Curr. Med. Chem. 10, 2643–2649.
Barman, K., Jasimuddin, Sk, 2014. RSC Adv. 4, 49819–49826.
Benvidi, A., Dehghani Firouzabadi, A., Dehghan Tezerjani, M., Moshtaghiun, S.M., Mazloum-Ardakani, M., Ansarin, A., 2015. J. Electroanal. Chem. 750, 57–64.
Bouffier, L., Gosse, I., Demeunynck, M., Mailley, P., 2012. Bioelectrochemistry 88, 103–109.
Brett, A.M.O., da Silva, L.A., Fujii, H., Mataka, S., Thiemann, T., 2003. J. Electroanal. Chem. 549, 91–99.
Cadet, J., Wagner, J.R., 2013. Cold Spring Harb. Perspect. Biol. 5 (2), a012559.
Cambridge Crystallographic Data Centre, 2015. GOLD User Guide A Component of the GOLD Suite. 245. ⟨https://www.ccdc.cam.ac.uk⟩.
Cholewiński, G., Dzierzbicka, K., Kołodziejczyk, A.M., 2011. Pharmacol. Rep. 63, 305–336.
Deng, Z., Hu, J., Liu, S., 2017. Macromol. Rapid Commun. 1600685.
Dogan-Topal, B., Bozal-Palabiyik, B., Ozkan, S.A., Uslu, B., 2014. Sens. Actuators B Chem. 194, 185–194.
Elias, B., Shao, F., Barton, J.K., 2008. J. Am. Chem. Soc. 130, 1152–1153.
Ferapontova, E.E., 2004. Electrochim. Acta 49, 1751–1759.
Gewald, K., 1965. Chem. Ber. 98, 3571–3577.
Gewald, K., Schinke, E., Böttcher, H., 1966. Chem. Ber. 99, 94–100.
Goodell, J.R., Madhok, A.A., Hiasa, H., Ferguson, D.M., 2006. Bioorg. Med. Chem. 14, 5467–5480.
Harbinder, S., Jatinder, V.S., Manish, K.G., Ajit, K.S., Sahil, S., Kunal, N., Preet, M.S.B., 2017. Bioorg. Med. Chem. Lett. 27, 3974–3979.
Huang, S., Lu, S., Huang, C., Sheng, J., Zhang, L., Su, W., Xiao, Q., 2016. Sens. Actuators B Chem. 224, 22–30.
Huang, Z., Lin, K., You, Q., 2013. Bioorg. Med. Chem. Lett. 23, 4166–4171.
Ibañez, D., Santidrian, A., Heras, A., Kalbáč, M., Colina, A., 2015. J. Phys. Chem. C 119, 8191–8198.
Kalanur, S.S., Katrahalli, U., Seetharamappa, J., 2009. J. Electroanal. Chem. 636, 93–100.
Kamal, A., Reddy, K.S., Khan, M.N.A., Shetti, R.V.C.R.N.C., Ramaiah, M.J., Pushpavalli, S.N.C.V.L., Srinivas, C., Pal-Bhadra, M., Chourasia, M., Sastry, G.N., Juvekar, A., Zingde, S., Barkume, M., 2010. Bioorg. Med. Chem. 18, 4747–4761.
Kovacic, P., Wakelin, L.P.G., 2001. Anti-Cancer Drug Des. 16, 175–184.
Kundu, P., Chattopadhyay, N., 2017. Photobiol. B Biol. 173, 485–492.
Labuda, J., Ovádeková, R., Galandová, J., 2009. Microchim. Acta 164, 371–377.
Lafayette, E.A., Vitalino de Almeida, S.M., Pitta, M.G., Carneiro Beltrão, E.I., da Silva, T.G., Olímpio de Moura, R., Pitta, I. a.R., de Carvalho, L.B., de Lima, M. o.C., 2013. Molecules 18, 15035–15050.
Lai, R.Y., Walker, B., Stormberg, K., Zaitouna, A.J., Yang, W., 2013. Methods 64, 267–275.
Li, Q., Batchelor-McAuley, C., Compton, R.G., 2010. J. Phys. Chem. B 114, 7423–7428.
Liu, T., Barton, J.K., 2005. J. Am. Chem. Soc. 127, 10160–10161. https://doi.org/10.1021/ja053025c.
Lucarelli, F., Marrazza, G., Turner, A.P., Mascini, M., 2004. Biosens. Bioelectron. 19, 515–530.
Lucarelli, F., Marrazza, G., Palchetti, I., Cesaretti, S., Mascini, M., 2002. Anal. Chim. Acta 469, 93–99.
McEwen, G.D., Chen, F., Zhou, A., 2009. Anal. Chim. Acta 643, 26–37.
Mills, D.M., Calvo-Marzal, P., Pinzon, J.M., Armas, S., Kolpashchikov, D.M., Chumbimuni- Torres, K.Y., 2017. Electroanalysis 29, 873–879.
Murali, S.R.S., Siddhardha, S.R.S., Babu, R.D., Venketesh, S., Basavaraju, R., Rao, N.G., 2017. Acta Part A Mol. Biomol. Spectrosc. 180, 217–223.
Nguyen, B., Wilson, W.D., 2009. J. Phys. Chem. B. 113, 14329–14335.
Nepali, K., Sharma, S., Sharma, M., Bedi, P.M.S., Dhar, K.L., 2014. Eur. J. Med. Chem. 77, 422–487.
Noh, J., Kwon, B., Han, E., Park, M., Yang, W., Cho, W., Yoo, W., Khang, G., Lee, D., 2015. Nat. Commun. 6, 6907.
Oliveira, S.C.B., Oliveira-Brett, A.M., 2010. Comb. Chem. High. Throughput Screen. 13, 628–640.
Paleček, E., Fojta, M., Tomschik, M., Wang, J., 1998. Biosens. Bioelectron. 13, 621–628.
Pontinha, A.D.R., Sparapani, S., Neidle, S., Oliveira-Brett, A.M., 2013. Bioelectrochemistry 89, 50–56.
Putic, A., Stecher, L., Prinz, H., Müller, K., 2010. Eur. J. Med. Chem. 45, 3299–3310.
Rauf, S., Gooding, J.J., Akhtar, K., Ghauri, M.A., Rahman, M., Anwar, M.A., Khalid, A.M., 2005. J. Pharm. Biomed. Anal. 37, 205–217.
Sazhnikov, V.A., Khlebunov, A.A., Sazonov, S.K., Vedernikov, A.I., Safonov, A.A., Bagatur'yants, A.A., Kuz'mina, L.G., Howard, J.A.K., Gromov, S.P., Alfimov, M.V., 2013. J. Mol. Struct. 1053, 79–88.
Silva-Júnior, E., França, P., Quintas-Júnior, L., Mendonça-Junior, F., Scotti, L., Scotti, M., de Aquino, T., Araújo-Júnior, J., 2017. Aided Drug Des. 13, 1–9.
Silva, M., Nascimiento, E.O., Edeildo, F.,M., 2017. Int. J. Biol. Macromol. 96, 223–233.
Silva, M., Savariz, F.C., Silva, E.F., De Aquino, T.M., Sarragiotto, M.H., Santos, J.C.C., Figueiredo, I.M., 2016. J. Braz. Chem. Soc. 27, 1558–1568.
Sirajuddin, M., Ali, S., Badshah, A., 2013. J. Photochem. Photobiol. B Biol. 124, 1–19.
Veerashekhar Goud, E., Sivaramakrishna, A., Vijayakrishna, K., Brahmmananda Rao, C.V.S., Khedkar, V.M., Jha, P.C., 2017. Inorg. Chim. Acta 461, 84–91.
Vyskočil, V., Labuda, J., Barek, J., 2010. Anal. Bioanal. Chem. 397, 233–241.
Wei, Y., Huang, Q.A., Li, M.G., Huang, X.J., Fang, B., Wang, L., 2011. Electrochim. Acta 56, 8571–8575.
Wong, E., Gooding, J., 2006. Anal. Chem. 78, 2138–2144.